

Soft and hard interactions in $p\bar{p}$ collisions at $\sqrt{s} = 1800$ and 630 GeV

D. Acosta,¹² T. Affolder,²³ H. Akimoto,⁴⁵ M. G. Albrow,¹¹ P. Amaral,⁸ D. Ambrose,³² D. Amidei,²⁵ K. Anikeev,²⁴ J. Antos,¹ G. Apollinari,¹¹ T. Arisawa,⁴⁵ A. Artikov,⁹ T. Asakawa,⁴³ W. Ashmanskas,⁸ F. Azfar,³⁰ P. Azzi-Bacchetta,³¹ N. Bacchetta,³¹ H. Bachacou,²³ S. Bailey,¹⁶ P. de Barbaro,³⁶ A. Barbaro-Galtieri,²³ V. E. Barnes,³⁵ B. A. Barnett,¹⁹ S. Baroiant,⁵ M. Barone,¹³ G. Bauer,²⁴ F. Bedeschi,³³ S. Belforte,⁴² W. H. Bell,¹⁵ G. Bellettini,³³ J. Bellinger,⁴⁶ D. Benjamin,¹⁰ J. Bensinger,⁴ A. Beretvas,¹¹ J. P. Berge,¹¹ J. Berryhill,⁸ A. Bhatti,³⁷ M. Binkley,¹¹ D. Bisello,³¹ M. Bishai,¹¹ R. E. Blair,² C. Blocker,⁴ K. Bloom,²⁵ B. Blumenfeld,¹⁹ S. R. Blusk,³⁶ A. Bocci,³⁷ A. Bodek,³⁶ G. Bolla,³⁵ Y. Bonushkin,⁶ D. Bortoletto,³⁵ J. Boudreau,³⁴ A. Brandl,²⁷ S. van den Brink,¹⁹ C. Bromberg,²⁶ M. Brozovic,¹⁰ E. Brubaker,²³ N. Bruner,²⁷ E. Buckley-Geer,¹¹ J. Budagov,⁹ H. S. Budd,³⁶ K. Burkett,¹⁶ G. Busetto,³¹ A. Byon-Wagner,¹¹ K. L. Byrum,² S. Cabrera,¹⁰ P. Calafiura,²³ M. Campbell,²⁵ W. Carithers,²³ J. Carlson,²⁵ D. Carlsmith,⁴⁶ W. Caskey,⁵ A. Castro,³ D. Cauz,⁴² A. Cerri,³³ A. W. Chan,¹ P. S. Chang,¹ P. T. Chang,¹ J. Chapman,²⁵ C. Chen,³² Y. C. Chen,¹ M.-T. Cheng,¹ M. Chertok,⁵ G. Chiarelli,³³ I. Chirikov-Zorin,⁹ G. Chlachidze,⁹ F. Chlebana,¹¹ L. Christofek,¹⁸ M. L. Chu,¹ J. Y. Chung,²⁸ Y. S. Chung,³⁶ C. I. Ciobanu,²⁸ A. G. Clark,¹⁴ A. P. Colijn,¹¹ A. Connolly,²³ M. Convery,³⁷ J. Conway,³⁸ M. Cordelli,¹³ J. Cranshaw,⁴⁰ R. Culbertson,¹¹ D. Dagenhart,⁴⁴ S. D'Auria,¹⁵ F. DeJongh,¹¹ S. Dell'Agnello,¹³ M. Dell'Orso,³³ S. Demers,³⁶ L. Demortier,³⁷ M. Deninno,³ P. F. Derwent,¹¹ T. Devlin,³⁸ J. R. Dittmann,¹¹ A. Dominguez,²³ S. Donati,³³ J. Done,³⁹ M. D'Onofrio,³³ T. Dorigo,¹⁶ N. Eddy,¹⁸ K. Einsweiler,²³ J. E. Elias,¹¹ E. Engels, Jr.,³⁴ R. Erbacher,¹¹ D. Errede,¹⁸ S. Errede,¹⁸ Q. Fan,³⁶ H.-C. Fang,²³ R. G. Feild,⁴⁷ J. P. Fernandez,¹¹ C. Ferretti,³³ R. D. Field,¹² I. Fiori,³ B. Flaughner,¹¹ G. W. Foster,¹¹ M. Franklin,¹⁶ J. Freeman,¹¹ J. Friedman,²⁴ Y. Fukui,²² I. Furic,²⁴ S. Galeotti,³³ A. Gallas,^{16,*} M. Gallinaro,³⁷ T. Gao,³² M. Garcia-Sciveres,²³ A. F. Garfinkel,³⁵ P. Gatti,³¹ C. Gay,⁴⁷ D. W. Gerdes,²⁵ P. Giannetti,³³ P. Giromini,¹³ V. Glagolev,⁹ D. Glenzinski,¹¹ M. Gold,²⁷ J. Goldstein,¹¹ I. Gorelov,²⁷ A. T. Goshaw,¹⁰ Y. Gotra,³⁴ K. Goulianos,³⁷ C. Green,³⁵ G. Grim,⁵ P. Gris,¹¹ C. Grosso-Pilcher,⁸ M. Guenther,³⁵ G. Guillian,²⁵ J. Guimaraes da Costa,¹⁶ R. M. Haas,¹² C. Haber,²³ S. R. Hahn,¹¹ C. Hall,¹⁶ T. Handa,¹⁷ R. Handler,⁴⁶ W. Hao,⁴⁰ F. Happacher,¹³ K. Hara,⁴³ A. D. Hardman,³⁵ R. M. Harris,¹¹ F. Hartmann,²⁰ K. Hatakeyama,³⁷ J. Hauser,⁶ J. Heinrich,³² A. Heiss,²⁰ M. Herndon,¹⁹ C. Hill,⁵ A. Hocker,³⁶ K. D. Hoffman,³⁵ R. Hollebeek,³² L. Holloway,¹⁸ B. T. Huffman,³⁰ R. Hughes,²⁸ J. Huston,²⁶ J. Huth,¹⁶ H. Ikeda,⁴³ J. Incandela,^{11,†} G. Introzzi,³³ A. Ivanov,³⁶ J. Iwai,⁴⁵ Y. Iwata,¹⁷ E. James,²⁵ M. Jones,³² U. Joshi,¹¹ H. Kambara,¹⁴ T. Kamon,³⁹ T. Kaneko,⁴³ M. Karagoz Unel,^{39,*} K. Karr,⁴⁴ S. Kartal,¹¹ H. Kasha,⁴⁷ Y. Kato,²⁹ T. A. Keaffaber,³⁵ K. Kelley,²⁴ M. Kelly,²⁵ D. Khazins,¹⁰ T. Kikuchi,⁴³ B. Kilminster,³⁶ B. J. Kim,²¹ D. H. Kim,²¹ H. S. Kim,¹⁸ M. J. Kim,²¹ S. B. Kim,²¹ S. H. Kim,⁴³ Y. K. Kim,²³ M. Kirby,¹⁰ M. Kirk,⁴ L. Kirsch,⁴ S. Klimenko,¹² P. Koehn,²⁸ K. Kondo,⁴⁵ J. Konigsberg,¹² A. Korn,²⁴ A. Korytov,¹² E. Kovacs,² J. Kroll,³² M. Kruse,¹⁰ S. E. Kuhlmann,² K. Kurino,¹⁷ T. Kuwabara,⁴³ A. T. Laasanen,³⁵ N. Lai,⁸ S. Lami,³⁷ S. Lammel,¹¹ J. Lancaster,¹⁰ M. Lancaster,²³ R. Lander,⁵ A. Lath,³⁸ G. Latino,³³ T. LeCompte,² K. Lee,⁴⁰ S. Leone,³³ J. D. Lewis,¹¹ M. Lindgren,⁶ T. M. Liss,¹⁸ J. B. Liu,³⁶ Y. C. Liu,¹ D. O. Litvintsev,¹¹ O. Lobban,⁴⁰ N. S. Lockyer,³² J. Loken,³⁰ M. Loreti,³¹ D. Lucchesi,³¹ P. Lukens,¹¹ S. Lusin,⁴⁶ L. Lyons,³⁰ J. Lys,²³ R. Madrak,¹⁶ K. Maeshima,¹¹ P. Maksimovic,¹⁶ L. Malferrari,³ M. Mangano,³³ M. Mariotti,³¹ G. Martignon,³¹ A. Martin,⁴⁷ J. A. J. Matthews,²⁷ P. Mazzanti,³ K. S. McFarland,³⁶ P. McIntyre,³⁹ M. Menguzzato,³¹ A. Menzione,³³ P. Merkel,¹¹ C. Mesropian,³⁷ A. Meyer,¹¹ T. Miao,¹¹ R. Miller,²⁶ J. S. Miller,²⁵ H. Minato,⁴³ S. Miscetti,¹³ M. Mishina,²² G. Mitselmakher,¹² Y. Miyazaki,²⁹ N. Moggi,³ E. Moore,²⁷ R. Moore,²⁵ Y. Morita,²² T. Moulik,³⁵ M. Mulhearn,²⁴ A. Mukherjee,¹¹ T. Muller,²⁰ A. Munar,³³ P. Murat,¹¹ S. Murgia,²⁶ J. Nachtman,⁶ V. Nagaslaev,⁴⁰ S. Nahn,⁴⁷ H. Nakada,⁴³ I. Nakano,¹⁷ C. Nelson,¹¹ T. Nelson,¹¹ C. Neu,²⁸ D. Neuberger,²⁰ C. Newman-Holmes,¹¹ C.-Y. P. Ngan,²⁴ H. Niu,⁴ L. Nodulman,² A. Nomerotski,¹² S. H. Oh,¹⁰ Y. D. Oh,²¹ T. Ohmoto,¹⁷ T. Ohsugi,¹⁷ R. Oishi,⁴³ T. Okusawa,²⁹ J. Olsen,⁴⁶ W. Orejudos,²³ C. Pagliarone,³³ F. Palmonari,³³ R. Paoletti,³³ V. Papadimitriou,⁴⁰ D. Partos,⁴ J. Patrick,¹¹ G. Pauletta,⁴² M. Paulini,^{23,‡} C. Paus,²⁴ D. Pellett,⁵ L. Pescara,³¹ T. J. Phillips,¹⁰ G. Piacentino,³³ K. T. Pitts,¹⁸ A. Pompos,³⁵ L. Pondrom,⁴⁶ G. Pope,³⁴ F. Prokoshin,⁹ J. Proudfoot,² F. Ptohos,¹³ O. Pukhov,⁹ G. Punzi,³³ A. Rakitine,²⁴ F. Ratnikov,³⁸ D. Reher,²³ A. Reichold,³⁰ P. Renton,³⁰ A. Ribon,³¹ W. Riegler,¹⁶ F. Rimondi,³ L. Ristori,³³ M. Riveline,⁴¹ W. J. Robertson,¹⁰ T. Rodrigo,⁷ S. Rolli,⁴⁴ L. Rosenson,²⁴ R. Roser,¹¹ R. Rossin,³¹ C. Rott,³⁵ A. Roy,³⁵ A. Ruiz,⁷ A. Safonov,⁵ R. St. Denis,¹⁵ W. K. Sakumoto,³⁶ D. Saltzberg,⁶ C. Sanchez,²⁸ A. Sansoni,¹³ L. Santi,⁴² H. Sato,⁴³ P. Savard,⁴¹ A. Savoy-Navarro,¹¹ P. Schlabach,¹¹ E. E. Schmidt,¹¹ M. P. Schmidt,⁴⁷ M. Schmitt,^{16,*} L. Scodellaro,³¹ A. Scott,⁶ A. Scribano,³³ A. Sedov,³⁵ S. Segler,¹¹ S. Seidel,²⁷ Y. Seiya,⁴³ A. Semenov,⁹ F. Semeria,³ T. Shah,²⁴ M. D. Shapiro,²³ P. F. Shepard,³⁴ T. Shibayama,⁴³ M. Shimojima,⁴³ M. Shochet,⁸ A. Sidoti,³¹ J. Siegrist,²³ A. Sill,⁴⁰ P. Sinervo,⁴¹ P. Singh,¹⁸ A. J. Slaughter,⁴⁷ K. Sliwa,⁴⁴ C. Smith,¹⁹ F. D. Snider,¹¹ A. Solodsky,³⁷ J. Spalding,¹¹ T. Speer,¹⁴ P. Sphicas,²⁴ F. Spinella,³³ M. Spiropulu,⁸ L. Spiegel,¹¹ J. Steele,⁴⁶ A. Stefanini,³³ J. Strologas,¹⁸ F. Strumia,¹⁴ D. Stuart,¹¹ K. Sumorok,²⁴ T. Suzuki,⁴³ T. Takano,²⁹ R. Takashima,¹⁷ K. Takikawa,⁴³ P. Tamburello,¹⁰ M. Tanaka,⁴³ B. Tannenbaum,⁶ M. Tecchio,²⁵ R. J. Tesarek,¹¹ P. K. Teng,¹ K. Terashi,³⁷ S. Tether,²⁴ A. S. Thompson,¹⁵ E. Thomson,²⁸ R. Thurman-Keup,² P. Tipton,³⁶ S. Tkaczyk,¹¹ D. Toback,³⁹ K. Tollefson,³⁶ A. Tollestrup,¹¹ D. Tonelli,³³ H. Toyoda,²⁹ W. Trischuk,⁴¹ J. F. de Troconiz,¹⁶ J. Tseng,²⁴ D. Tsybychev,¹¹ N. Turini,³³ F. Ukegawa,⁴³ T. Vaiculis,³⁶ J. Valls,³⁸ S. Vejcik III,¹¹ G. Velev,¹¹ G. Veramendi,²³ R. Vidal,¹¹ I. Vila,⁷ R. Vilar,⁷ I. Volobouev,²³ M. von der Mey,⁶ D. Vucinic,²⁴ R. G. Wagner,² R. L. Wagner,¹¹ N. B. Wallace,³⁸ Z. Wan,³⁸ C. Wang,¹⁰ M. J. Wang,¹ S. M. Wang,¹² B. Ward,¹⁵ S. Waschke,¹⁵ T. Watanabe,⁴³ D. Waters,³⁰ T. Watts,³⁸ R. Webb,³⁹ H. Wenzel,²⁰ W. C. Wester III,¹¹ A. B. Wicklund,² E. Wicklund,¹¹ T. Wilkes,⁵ H. H. Williams,³² P. Wilson,¹¹

B. L. Winer,²⁸ D. Winn,²⁵ S. Wolbers,¹¹ D. Wolinski,²⁵ J. Wolinski,²⁶ S. Wolinski,²⁵ S. Worm,³⁸ X. Wu,¹⁴ J. Wyss,³³
 W. Yao,²³ G. P. Yeh,¹¹ P. Yeh,¹ J. Yoh,¹¹ C. Yosef,²⁶ T. Yoshida,²⁹ I. Yu,²¹ S. Yu,³² Z. Yu,⁴⁷ A. Zanetti,⁴² F. Zetti,²³
 and S. Zucchelli³

(CDF Collaboration)

- ¹*Institute of Physics, Academia Sinica, Taipei, Taiwan 11529, Republic of China*
²*Argonne National Laboratory, Argonne, Illinois 60439*
³*Istituto Nazionale di Fisica Nucleare, University of Bologna, I-40127 Bologna, Italy*
⁴*Brandeis University, Waltham, Massachusetts 02254*
⁵*University of California at Davis, Davis, California 95616*
⁶*University of California at Los Angeles, Los Angeles, California 90024*
⁷*Instituto de Fisica de Cantabria, CSIC–University of Cantabria, 39005 Santander, Spain*
⁸*Enrico Fermi Institute, University of Chicago, Chicago, Illinois 60637*
⁹*Joint Institute for Nuclear Research, RU-141980 Dubna, Russia*
¹⁰*Duke University, Durham, North Carolina 27708*
¹¹*Fermi National Accelerator Laboratory, Batavia, Illinois 60510*
¹²*University of Florida, Gainesville, Florida 32611*
¹³*Laboratori Nazionali di Frascati, Istituto Nazionale di Fisica Nucleare, I-00044 Frascati, Italy*
¹⁴*University of Geneva, CH-1211 Geneva 4, Switzerland*
¹⁵*Glasgow University, Glasgow G12 8QQ, United Kingdom*
¹⁶*Harvard University, Cambridge, Massachusetts 02138*
¹⁷*Hiroshima University, Higashi-Hiroshima 724, Japan*
¹⁸*University of Illinois, Urbana, Illinois 61801*
¹⁹*The Johns Hopkins University, Baltimore, Maryland 21218*
²⁰*Institut für Experimentelle Kernphysik, Universität Karlsruhe, 76128 Karlsruhe, Germany*
²¹*Center for High Energy Physics, Kyungpook National University, Taegu 702-701, Korea, Seoul National University, Seoul 151-742, Korea, and SungKyunKwan University, Suwon 440-746, Korea*
²²*High Energy Accelerator Research Organization (KEK), Tsukuba, Ibaraki 305, Japan*
²³*Ernest Orlando Lawrence Berkeley National Laboratory, Berkeley, California 94720*
²⁴*Massachusetts Institute of Technology, Cambridge, Massachusetts 02139*
²⁵*University of Michigan, Ann Arbor, Michigan 48109*
²⁶*Michigan State University, East Lansing, Michigan 48824*
²⁷*University of New Mexico, Albuquerque, New Mexico 87131*
²⁸*The Ohio State University, Columbus, Ohio 43210*
²⁹*Osaka City University, Osaka 588, Japan*
³⁰*University of Oxford, Oxford OX1 3RH, United Kingdom*
³¹*Universita di Padova, Istituto Nazionale di Fisica Nucleare, Sezione di Padova, I-35131 Padova, Italy*
³²*University of Pennsylvania, Philadelphia, Pennsylvania 19104*
³³*Istituto Nazionale di Fisica Nucleare, University and Scuola Normale Superiore of Pisa, I-56100 Pisa, Italy*
³⁴*University of Pittsburgh, Pittsburgh, Pennsylvania 15260*
³⁵*Purdue University, West Lafayette, Indiana 47907*
³⁶*University of Rochester, Rochester, New York 14627*
³⁷*Rockefeller University, New York, New York 10021*
³⁸*Rutgers University, Piscataway, New Jersey 08855*
³⁹*Texas A&M University, College Station, Texas 77843*
⁴⁰*Texas Tech University, Lubbock, Texas 79409*
⁴¹*Institute of Particle Physics, University of Toronto, Toronto, Canada M5S 1A7*
⁴²*Istituto Nazionale di Fisica Nucleare, University of Trieste/Udine, Italy*
⁴³*University of Tsukuba, Tsukuba, Ibaraki 305, Japan*
⁴⁴*Tufts University, Medford, Massachusetts 02155*
⁴⁵*Waseda University, Tokyo 169, Japan*
⁴⁶*University of Wisconsin, Madison, Wisconsin 53706*
⁴⁷*Yale University, New Haven, Connecticut 06520*
 (Received 26 October 2001; published 5 April 2002)

We present a study of $p\bar{p}$ collisions at $\sqrt{s}=1800$ and 630 GeV collected using a minimum bias trigger by the CDF experiment in which the data set is divided into two classes corresponding to “soft” and “hard” interactions. For each subsample, the analysis includes measurements of the multiplicity, transverse momentum (p_T) spectrum, and the average p_T and event-by-event p_T dispersion as a function of multiplicity. A comparison of results shows distinct differences in the behavior of the two samples as a function of the center of mass (c.m.) energy. We find evidence that the properties of the *soft* sample are invariant as a function of c.m. energy.

DOI: 10.1103/PhysRevD.65.072005

PACS number(s): 13.85.Hd, 12.38.Mh, 13.87.Fh

I. INTRODUCTION

Hadron interactions are often classified as either “hard” or “soft” [1,2]. Although there is no formal definition for either, the term “hard interactions” is typically understood to mean high transverse energy (E_T) parton-parton interactions associated with such phenomena as high E_T jets, while the soft component consists of everything else. Whereas perturbative QCD provides a reasonable description of high E_T jet production, there is no equivalent theory for the low E_T multiparticle production processes that dominate the inelastic cross section. Some QCD inspired models [2] attempt to describe these processes by the superposition of many parton interactions extrapolated to very low momentum transfers. It is not known, however, if such a superposition or some collective multiparton process is at work.

The study of low- E_T interactions usually involves collecting data using minimum bias (MB) triggers, which, ideally, sample events in fixed proportion to the production rate—in other words, in their “natural” distribution. Lacking a comprehensive description of the microscopic processes [3] involved in low- E_T interactions, our knowledge of the details of low transverse momentum (p_T) particle production rests largely upon empirical connections between phenomenological models and data collected with MB triggers at many center-of-mass (c.m.) energies. Such comparisons are further complicated by the difficulty in isolating events of a purely “soft” or purely “hard” nature.

This paper adopts a novel approach in addressing this issue using samples of $p\bar{p}$ collisions at $\sqrt{s}=1800$ and 630 GeV collected with a MB trigger. The analysis first divides the full minimum bias samples into two subsamples, one highly enriched in soft interactions, the other relatively depleted of soft interactions. We then compare inclusive distributions and final state correlations between the subsamples and as a function of c.m. energy in order to gain insight into the mechanisms of particle production in soft interactions. The results in the isolated soft sample exhibit some interesting properties, in particular an unpredicted invariance with c.m. energy.

II. DATA SET AND EVENT SELECTION

Data samples have been collected with the Collider Detector at Fermilab (CDF) experiment at the Fermilab Teva-

tron Collider. The CDF apparatus has been described elsewhere [4]; here only the parts of the detector utilized for the present analysis are discussed.

Data at 1800 GeV were collected with a minimum bias trigger during runs 1A and 1B, and at 1800 and 630 GeV during run 1C. This trigger requires coincident hits in scintillator counters located at 5.8 m on either side of the nominal interaction point and covering the pseudo-rapidity [$\eta = -\log(\tan(\theta/2))$ where $\theta =$ angle with respect to the proton direction] interval $3.2 < |\eta| < 5.9$, in coincidence with a beam-crossing signal.

The analysis uses charged tracks reconstructed within the central tracking chamber (CTC). The CTC is a cylindrical drift chamber covering a η interval of about three units with full efficiency for $|\eta| \leq 1$ and $p_T \geq 0.4$ GeV/ c .

The inner radius of the CTC is 31.0 cm and the outer radius is 132.5 cm. The full CTC volume is contained in the superconducting solenoidal magnet which operates at 1.4 T [5]. The CTC has 84 sampling wire layers, organized in 5 axial and 4 stereo “superlayers” [6]. Axial superlayers have 12 radially separated layers of sense wires, parallel to the z axis (the beam axis), that measure the r - ϕ position of a track. Stereo superlayers have 6 sense wire layers, with an $\sim 3^\circ$ stereo angle, that measure a combination of r - ϕ and z information. The stereo angle direction alternates at each stereo superlayer. Axial and stereo data are combined to form a three-dimensional track.

The spatial resolution of each point measurement in the CTC is less than 200 μm ; the transverse momentum resolution, including multiple scattering effects, is $\sigma_{p_T}/p_T^2 \leq 0.003$ (GeV/ c).

Inside the CTC inner radius, a set of time projection chambers (VTX) [7] provides r - z tracking information out to a radius of 22 cm for $|\eta| < 3.25$. The VTX is used in this analysis to find the z position of event vertices, defined as a set of tracks with p_T greater than about 50 MeV/ c that converge to the same point along the z axis. Reconstructed vertices are classified as either “primary” or “secondary” based upon several parameters: the number of converging track segments (with a minimum of four within $|\eta| < 3$), the total number of hits used to form a segment, forward-backward symmetry and vertex isolation. Isolated, higher multiplicity vertices with highly symmetric topologies are typically classified as primary; lower multiplicity, highly asymmetric vertices or those with few hits in the reconstructed tracks are typically classified as secondary. Systematic uncertainties introduced by the vertex classification scheme are discussed in Sec. VI.

The transverse energy flux was measured by a calorimeter

*Now at Northwestern University, Evanston, IL 60208.

†Now at University of California, Santa Barbara, CA 93106.

‡Now at Carnegie Mellon University, Pittsburgh, PA 15213.

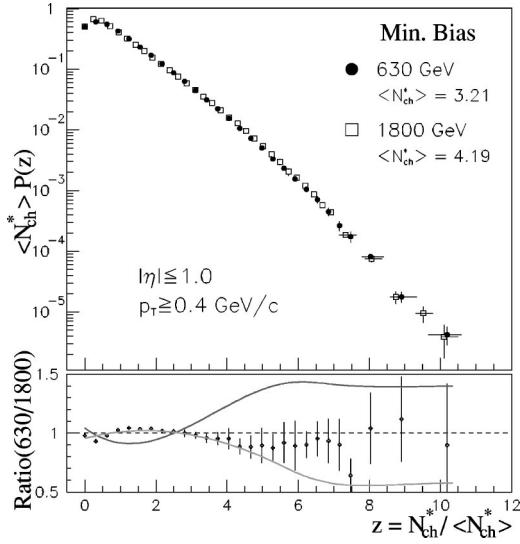


FIG. 1. Multiplicity distributions for the full MB samples at 1800 and 630 GeV; data are plotted in KNO variables. In the bottom panel the ratio of the two above distributions is shown. The two continuous lines delimit the band of all systematic uncertainties (see Sec. VI of text).

system [8] covering from -4.2 to 4.2 in η . The system consists of three subsystems, each with separate electromagnetic and hadronic compartments: the central calorimeter, covering the range $|\eta| < 1$; the end-plug, covering $1 < |\eta| < 2.4$; and the forward calorimeter, covering $2.2 < |\eta| < 4.2$. Energy measurements are made within projective “towers” that span 0.1 units of η and 15° in azimuth (ϕ) within the central calorimeter, and 5° in the end-plug and forward calorimeters.

The 1800 GeV data sample consists of subsamples collected during three different time periods. Approximately 1 700 000 events were collected in run 1A at an average luminosity of $3.3 \times 10^{30} \text{ s}^{-1} \text{ cm}^{-2}$, 1 500 000 in run 1B at an

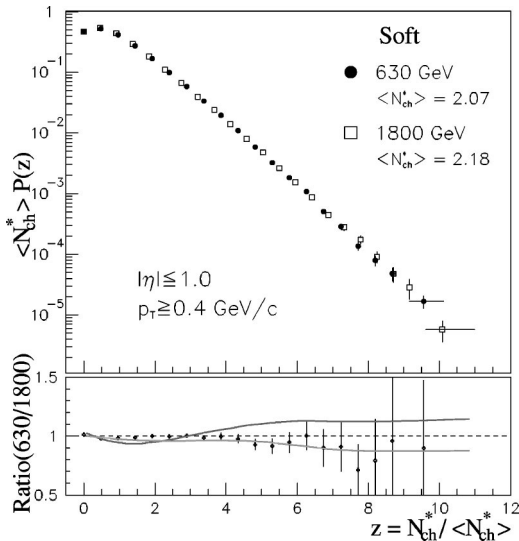


FIG. 2. Same as Fig. 1 for the *soft* samples.

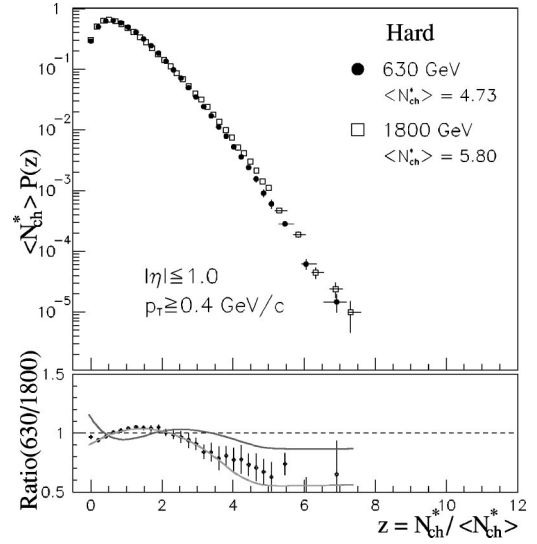


FIG. 3. Same as Fig. 1 for the *hard* samples.

average luminosity of $9.1 \times 10^{30} \text{ s}^{-1} \text{ cm}^{-2}$ and 106 000 in run 1C at an average luminosity of $9.0 \times 10^{30} \text{ s}^{-1} \text{ cm}^{-2}$. The 630 GeV data set consists of about 2 600 000 events recorded during run 1C at an average luminosity of $1.3 \times 10^{30} \text{ s}^{-1} \text{ cm}^{-2}$.

Additional event selection conducted offline removed the following events: (i) events identified as containing cosmic-ray particles as determined by time-of-flight measurements using scintillator counters in the central calorimeter; (ii) events with no reconstructed tracks; (iii) events exhibiting symptoms of known calorimeter problems; (iv) events with at least one charged particle reconstructed in the CTC

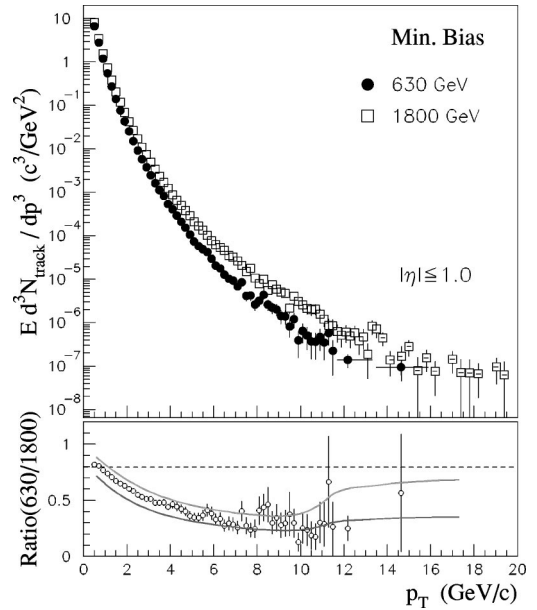


FIG. 4. Transverse momentum distributions for the full MB samples at 1800 and 630 GeV. In the bottom panel the ratio of the two distributions is shown. The two continuous lines delimit the band of all systematic uncertainties (see Sec. VI of text). N_{track} refers to the number of charged tracks in a unit η interval.

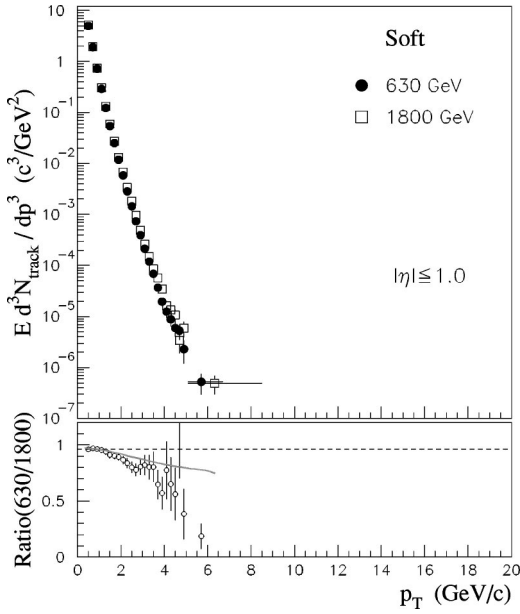


FIG. 5. Same as Fig. 4 for the *soft* samples. The continuous line in the ratio plot shows the upper limit of the systematic uncertainties. The lower limit overlaps the data points.

have $p_T \geq 400$ MeV/ c , but no central calorimeter tower with energy deposition above 100 MeV; (v) events with more than one primary vertex; (vi) events with a primary vertex more than 60 cm away from the center of the detector (in order to keep full tracking efficiency in the CTC and avoid energy leakage through exposed cracks in the calorimeter); (vii) events with no primary vertices.

After all event selection cuts, 2 079 558 events remain in the full minimum bias sample at $\sqrt{s} = 1800$ GeV (runs 1A + 1B + 1C), and 1 963 157 in that at $\sqrt{s} = 630$ GeV (run 1C).

The vast majority of rejected events failed the vertex selection. About 0.01% of selected events contain background tracks from cosmic rays that are coincident in time with the beam crossing and pass near the event vertex. The residual beam gas contamination is about 0.02%.

Section VI discusses the systematic uncertainties that arise from the event selection criteria and other sources.

III. TRACK SELECTION

Reconstructed tracks within each event must pass selection criteria designed to remove the main sources of background. Tracks must pass through a minimum number of layers in the CTC, and have a minimum number of hits in each superlayer in order to reduce the number of tracks with reconstruction errors. Fake and secondary particle tracks are removed by requiring that tracks pass within 0.5 cm off the beam axis, and within 5 cm along the z axis off the primary event vertex. Accepting only tracks with $p_T \geq 0.4$ GeV/ c and within $|\eta| \leq 1.0$ ensures full efficiency and acceptance.

We define the charged track multiplicity in an event, N_{ch}^* , as the number of selected CTC tracks in the event. The mean p_T of the event is defined as

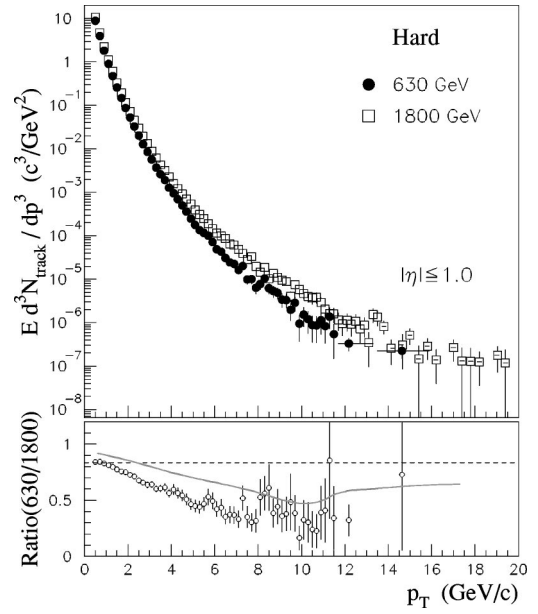


FIG. 6. Same as Fig. 4 for the *hard* samples. The continuous line in the ratio plot shows the upper limit of the systematic uncertainties. The lower limit overlaps the data points.

$$\bar{p}_T = \frac{1}{N_{ch}^*} \sum_i^{N_{ch}^*} p_{T_i} \quad (1)$$

unless stated otherwise.

IV. SELECTION OF *SOFT* AND *HARD* INTERACTIONS

The identification of “soft” and “hard” interactions is largely a matter of definition [9]. In this analysis we use a jet reconstruction algorithm to distinguish between the two classes. The algorithm employs a cone with radius $R = (\Delta\eta^2 + \Delta\phi^2)^{1/2} = 0.7$ to define “clusters” of calorimeter towers belonging to the jet. To be considered, a cluster must have a transverse energy (E_T) of at least 1 GeV in a seed tower, plus at least 0.1 GeV in an adjacent tower.

In the regions $|\eta| < 0.02$ and $1.1 < |\eta| < 1.2$, a track clustering algorithm is used instead of the calorimeter algorithm in order to compensate for energy lost in calorimeter cracks. A track cluster is defined as one track with $p_T > 0.7$ GeV/ c and at least one other track with $p_T \geq 0.4$ GeV/ c in a cone of radius $R = 0.7$.

We define a *soft* event as one that contains no cluster with $E_T > 1.1$ GeV. All other events are classified as *hard*.

V. EFFICIENCY CORRECTIONS

The track reconstruction efficiency for the CTC has been investigated for several different analyses and under various conditions at CDF [10–12]. For this analysis, we have calculated a full-event track reconstruction efficiency using a parametric Monte Carlo (MC) sample. Version 5.7 of the PYTHIA generator was used with the minimum bias configuration tuned to match the inclusive multiplicity and p_T distributions of the 1800 GeV sample (see the Appendix). For

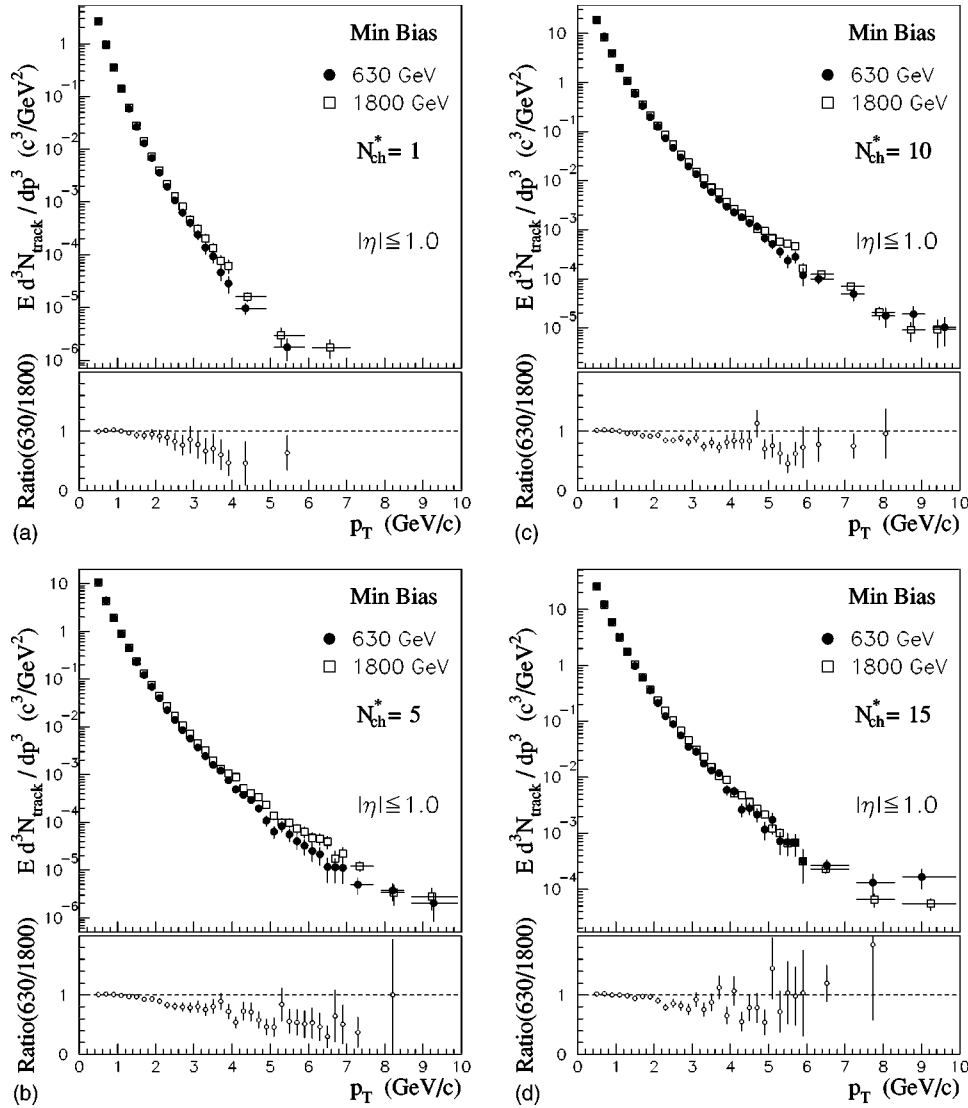


FIG. 7. Transverse momentum distributions at fixed multiplicity (multiplicity=1, 5, 10, 15) for the full MB samples at 1800 and 630 GeV. At the bottom of each plot the ratio of the two above distributions is shown. Error bars represent statistical error only. Systematic error was found to be negligible and is not included.

each inclusive distribution, a track finding efficiency correction was computed by taking the ratio of the PYTHIA generated distribution to the corresponding distribution from tracks traced through the apparatus. The efficiency for reconstructing the correct event charged multiplicity is about 95% up to a multiplicity of about 20, falling to about 85% at multiplicities above about 20.

The same PYTHIA MC sample was used to evaluate the background from gamma ray conversions, charged and neutral particle decays. Correction factors due to these effects have been computed as a function of track p_T and the event multiplicity.

There exists a small contamination from diffractive events even in the restricted region of phase space examined in this study. We have evaluated this contamination with a special PYTHIA MC run in which only the diffractive generation algorithm was switched on. The data were then subjected to the full event and track selection procedure. The correction for this effect is estimated to be about 5% in the zero multiplicity bin, decreasing rapidly to zero for $N_{ch}^* \sim 4$. In the p_T distribution, the correction is between zero and 1% up to about 1 GeV/c.

VI. SYSTEMATIC UNCERTAINTIES

Several sources of systematic errors have been investigated. The effect of each on the final distributions is discussed below.

Vertex selection. As discussed in Sec. II, the vertex selection classifies vertices as either “primary” or “secondary.” The standard selection demands that primary vertices be highly isolated. Misclassification or identification of vertices can strongly influence the p_T and multiplicity distributions, particularly the latter. We set conservative bounds on the magnitude of this effect in the following way. Two samples of events are selected. In one, all vertices except the highest quality one are classified as secondaries. In the other sample, all vertices are classified as primary. Compared to results obtained using the standard vertex selection, the ratio of the multiplicity distribution at $\sqrt{s}=630$ to that at 1800 GeV varies by about 5% in the region between a multiplicity of two and 11, and reaches 40% for multiplicities in excess of 22. The deviation in the ratio of p_T distributions at the two energies is almost constant at about 10% up to a p_T around 11 GeV/c, increasing to 15% as p_T increases.

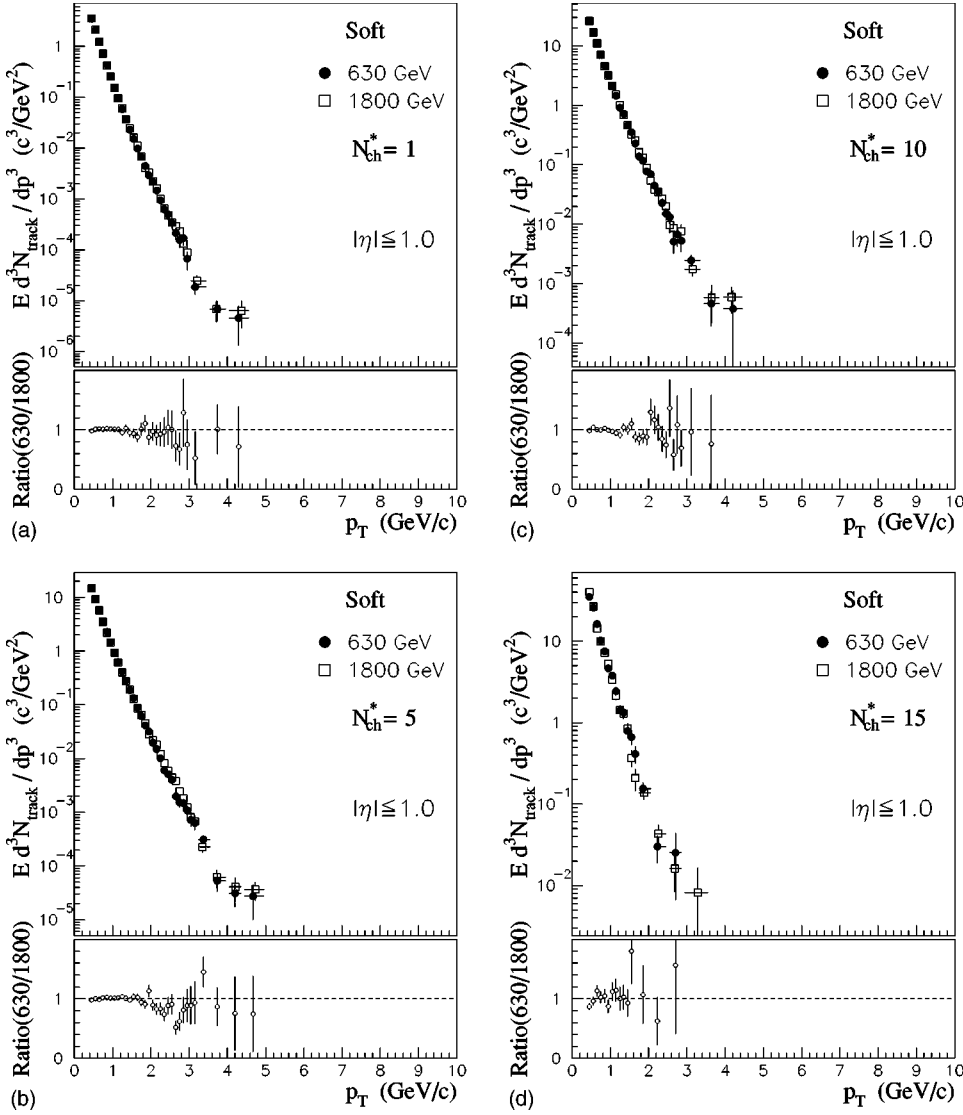


FIG. 8. Same as Fig. 4 for the *soft* samples.

Vertices in some multiple interaction events remain unresolved and introduce a residual luminosity-dependent contamination. We estimate the systematic uncertainty from this source by comparing the results of the complete analysis on two subsamples of data, one at low luminosity ($< 1.5 \times 10^{30} \text{ cm}^{-2} \text{ s}^{-1}$) and the other at high luminosity ($> 7 \times 10^{30} \text{ cm}^{-2} \text{ s}^{-1}$). Differences range between 2% and 6% for multiplicities less than 20, increasing to about 16% for multiplicities in the range $20 < N_{ch}^* < 30$, and to 45% for multiplicities greater than 30. The effect on the ratios of the various distributions is negligible.

The selection of events identified with known calorimeter problems depends upon thresholds applied to classify the anomalous behavior. This selection removes $\leq 1\%$ of the total sample. Changing the rejection factor causes no appreciable change in the distribution ratios.

Tracking efficiencies evaluated at CDF under various conditions and using different techniques obtain results that differ by as much as 8–10% in the low p_T (below 1 GeV/c), high p_T (above 2 GeV/c) or high multiplicity regions. The

impact of using widely different efficiency corrections on the multiplicity and p_T distributions is—at most—as large as the statistical uncertainty. The effect on the distribution ratios is negligible.

The systematic uncertainty due to the correction for gamma conversions, secondary particle interactions and particle decays is estimated to be about 1%, almost independent of multiplicity and p_T . The effect on the ratios of distributions is negligible.

The systematic uncertainty in the correction to the multiplicity distribution due to contamination from diffractive production is of the order of 1%, and limited to the very low multiplicities ($0 \leq N_{ch}^* \leq 3$). No correction was applied to the p_T distribution, where the magnitude of the effect was less than 1% for all p_T . The effect is negligible on the distribution ratios.

The systematic uncertainty from the vertex selection dominates all other sources. The curves on the final inclusive distribution ratios are obtained as the ratios of the distributions originated by the extreme selections outlined above.

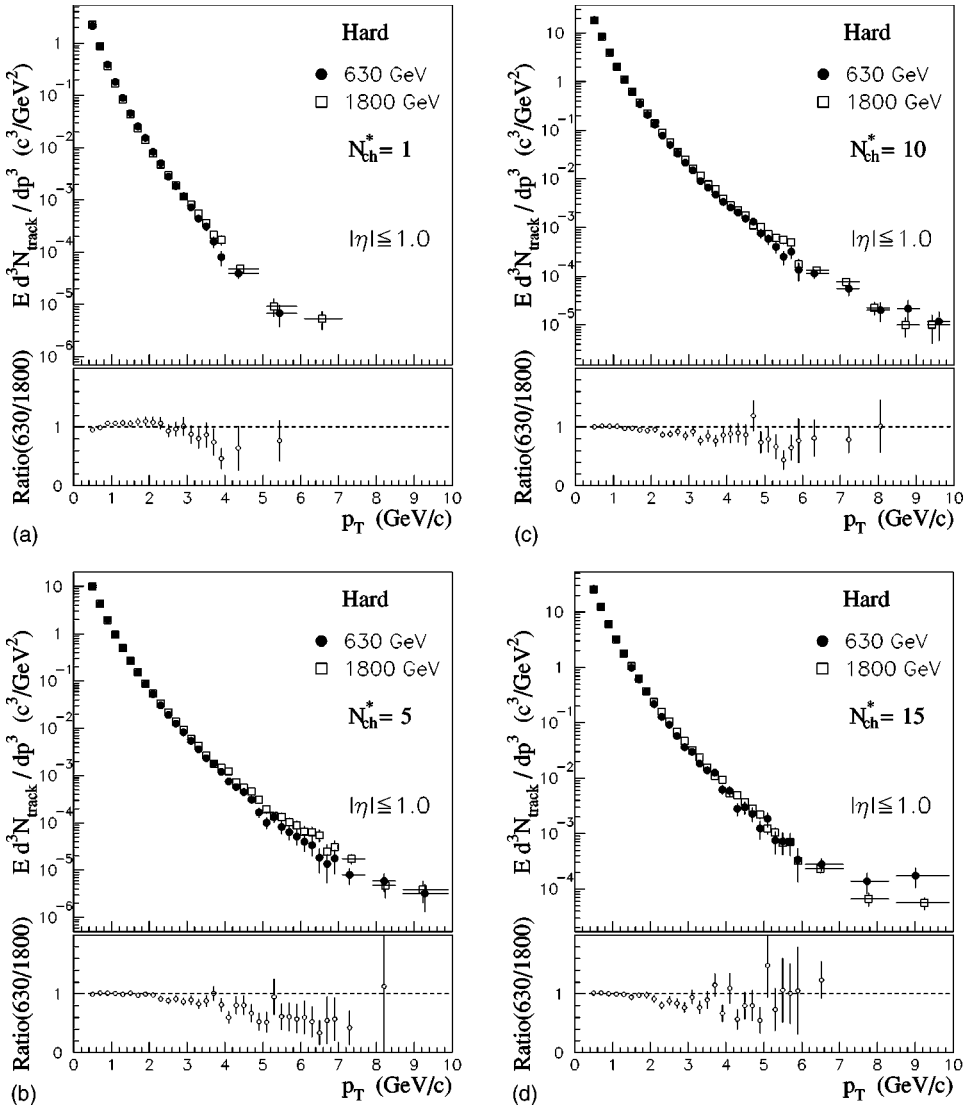


FIG. 9. Same as Fig. 4 for the *hard* samples.

They are not intended as point-to-point systematic uncertainties, but are included in the figures to show the approximate range over which the shape of the final distribution may be changed by altering the vertex selection.

Systematic effects cancel in the ratios of final state correlations (see Secs. VII B and VII C).

VII. DATA ANALYSIS

A. Inclusive distributions

We first examine the inclusive multiplicity and transverse momentum distributions. Figure 1 shows the multiplicity distributions for the full MB samples at 1800 and 630 GeV, plotted in Koba-Nielsen-Olesen (KNO)¹ variables [13]. The

¹Multiplicity distributions can be described in terms of the so-called KNO variables $\langle n \rangle P(n)$ and $z = n/\langle n \rangle$, where $P(n)$ is the probability for an event with n charged particles, and $\langle n \rangle$ is the average number of charged particles. “KNO scaling” implies the universal form for the multiplicity distribution $\langle n \rangle P(n) = \Psi(z)$, where $\Psi(z)$ is energy independent.

distributions at the two energies show a weak violation of KNO scaling, as it is expected in a limited phase space region [14]. The same comparison is made in Figs. 2 and 3 for the soft and hard samples separately. The ratio of the multiplicity distributions at the two energies are plotted at the bottom of Figs. 1, 2 and 3.

Transverse momentum distributions at the two energies are shown in Fig. 4 for the full MB sample. Figures 5 and 6 show the same distributions for the “soft” and “hard” sample, respectively. As for the multiplicity distributions, the ratios of the distributions at the two energies are shown in the bottom of these figures. The p_T spectrum in the soft sample falls more rapidly with increasing p_T than that of the hard sample. This difference is expected and reflects the absence of events with high p_T jets in the soft sample.

A deeper insight into the dynamics of the interactions can be gained by comparing the p_T distributions for *fixed* charged multiplicity as a function of \sqrt{s} . Figure 7 shows fixed-multiplicity p_T distributions for the full MB sample at the two energies superimposed. The same distributions are plotted in Figs. 8 and 9 for the soft and hard subsamples,

respectively. For brevity, only multiplicities of 1, 5, 10 and 15 are shown.

We observe that, within uncertainties, the p_T distributions for a given multiplicity are the same at $\sqrt{s}=1800$ and 630 GeV—they are c.m. energy invariant. None of the current models predict or suggest such an invariance. The result suggests that in purely soft interactions the number of produced (charged) particles is the only global event variable changing with \sqrt{s} . The particle multiplicity may also fix other event properties independently of the energy of the reaction.

A further observation is worth noting. It is known that for minimum bias samples, the slope of the inclusive p_T distribution increases steadily by some power of $\log s$ up to Tevatron energies [10,15]. Such an increase is also visible for p_T distributions at fixed multiplicity for the full MB sample shown in Fig. 7. The result of the present analysis implies that the \sqrt{s} dependence in the slope of the p_T distribution of the soft sample is due entirely to the change in the mean multiplicity. In contrast, the more pronounced change in the shape of the full MB and the hard samples as a function of \sqrt{s} must be caused in part by the increasing cross section of hard parton interactions.

B. Dependence of mean track p_T on charged multiplicity

The correlation between mean p_T and charged multiplicity was first observed by UA1 [16], and then investigated at the CERN Intersecting Storage Rings (ISR) [17] and Tevatron collider energies [15,18]. Although several different theoretical explanations have been proposed, such as geometrical models [19], thermodynamical models [20] and contributions from semihard parton scattering (minijets) [21], none provide satisfactory predictions for existing experimental results, leaving the real origin of the effect unexplained. Simulations performed with PYTHIA and HERWIG generators do not show better agreement with data (see Fig. 10) [22].

In this analysis the mean p_T (to be distinguished from the mean event p_T) is obtained by summing the p_T of all reconstructed charged tracks in all events with a given charged multiplicity, then dividing by the number of such tracks. The results are shown in Fig. 11 for the full minimum bias sample at the two analyzed energies, and in Figs. 12 and 13 for the *soft* and for the *hard* samples, respectively. The event multiplicity is smeared by track finding inefficiency. We correct the data points for the average track finding efficiency at each multiplicity.

The mean p_T as a function of multiplicity for the soft sample (Fig. 12) is nearly identical at the two energies. This invariance is a direct consequence and a confirmation of the invariance of the soft p_T spectra at fixed multiplicities noted in the previous section.

Comparing Figs. 12 and 13, we note a clear difference in the mean p_T correlation of the *soft* and *hard* samples. Interestingly, the mean p_T increases at low multiplicity even in the soft sample, which should be highly depleted in high E_T events. This observation suggests that an increasing contribution from hard gluon production, as proposed in Ref. [21],

is at least not the only mechanism responsible for the correlation at low multiplicity.

C. $\langle p_T \rangle_{ev}$ dispersion versus multiplicity

Event-by-event fluctuations of the mean event p_T have been shown to be a useful tool to investigate the collective behavior of soft multibody production, and has been used to analyze experimental data in various different ways [23–25]. Following the approach of [23], the dispersion, D_m , of the mean event p_T for events with multiplicity m ($m \equiv N_{ch}^*$) is defined as

$$D_m(\bar{p}_T) = \frac{\langle \bar{p}_T^2 \rangle_m - \langle \bar{p}_T \rangle_m^2}{\langle \bar{p}_T \rangle_{sample}^2}. \quad (2)$$

The angular brackets $\langle \rangle$ indicate an average over all events with the given multiplicity m , while \bar{p}_T is the mean event p_T from Eq. (1).

The dispersion is expected to decrease with increasing multiplicity and to converge to zero when $m \rightarrow \infty$ if only statistical fluctuations are present. Conversely, an extrapolation to a non-zero value would indicate the presence of non-statistical fluctuations in \bar{p}_T from event to event. This indeed is what was found in [23] and, in different ways, in Refs. [24] and [25]. Large non-statistical fluctuations of the mean event p_T are a consequence of particle correlations in the multibody final state [26]. Figure 14 shows the present measurement of the dispersion as a function of the inverse multiplicity for the full minimum bias samples. The correlation curve has a slope that varies across multiplicities, particularly at $\sqrt{s}=1800$ GeV. The dispersion versus inverse multiplicity for the soft and hard samples, shown in Figs. 15 and 16, confirms that this effect is related to the contribution of jet production which, as discussed in [27], increases event-by-event fluctuations. The plots show only statistical uncertainties.

Comparing our soft sample results with the full MB results of Ref. [23], where hard jet production has a much lower cross section than at Tevatron energies, we note that our points, unlike those in Ref. [23], cannot be interpolated with a straight line but show a steeper decrease in the region of high multiplicity (multiplicity ≥ 7). Since statistical fluctuations vary linearly with the multiplicity, this indicates that final state particle correlations change with multiplicity. Moreover, the results plotted in Fig. 15, although favoring a small positive value, are consistent with an extrapolation to zero at infinite multiplicity. These observations support the idea that asymptotically the event mean p_T has no dynamical fluctuations.²

Finally, the dispersion as a function of the inverse multiplicity for the soft samples has a constant ratio at the two energies, a fact which is not true for the hard samples.

²It has been observed [28] that this method cannot exclude the possibility of opposite sign correlations that perfectly cancel each other.

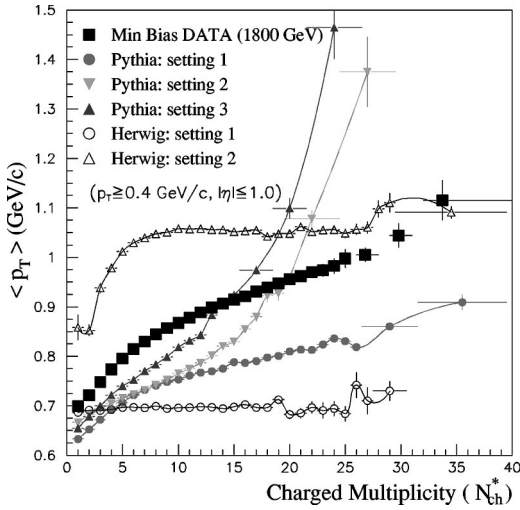


FIG. 10. Mean transverse momentum vs multiplicity from Monte Carlo. The different parameter settings for each MC generator are given in the Appendix.

VIII. DEPENDENCE ON E_T THRESHOLD

As noted in Sec. IV, the identification of soft and hard events is essentially a matter of definition. To investigate the sensitivity of our results to the details of the selection criteria, we repeated the analysis using a transverse energy threshold of 3 GeV instead of 1.1 GeV on the energy cluster definition. Although, as expected, the higher threshold value strongly influences the inclusive distributions, it does not substantially change the characteristic differences between the soft and hard samples. In particular, it preserves the energy invariance of the soft sample distributions and correlations. This can be seen in Fig. 17 where the ratios of multiplicity, mean p_T correlation and dispersion between the two

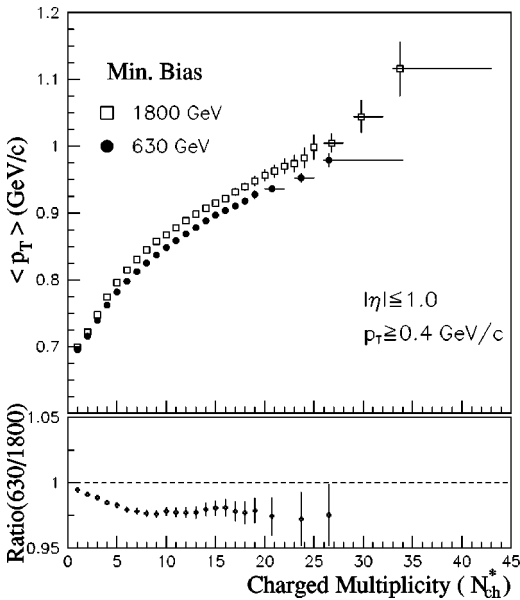


FIG. 11. Mean transverse momentum vs multiplicity for the full MB samples at 1800 and 630 GeV. On the bottom the ratio of the two curves is shown.

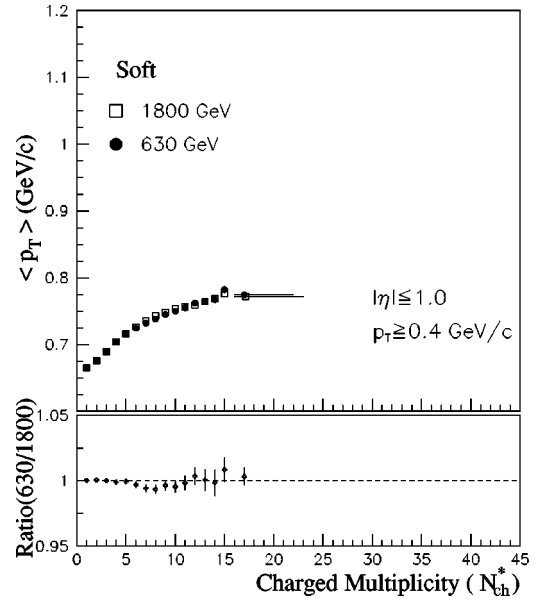


FIG. 12. Same as Fig. 11 for the *soft* samples.

energies are compared for the two different threshold choices.

IX. CONCLUSIONS

Assuming that hard parton interactions in $\bar{p}p$ scattering eventually develop into final state particles observable as clustered within jet cones, and pushing the cluster identification threshold as low as possible, we separate minimum bias events into subsamples enriched in soft or hard collisions. Comparing the behavior of the two samples at two energies, we obtain the following results.

The multiplicity distributions of “soft” interactions follow KNO scaling going from $\sqrt{s} = 630$ to 1800 GeV. This is not true for those of the “hard” subsample. The p_T distribu-

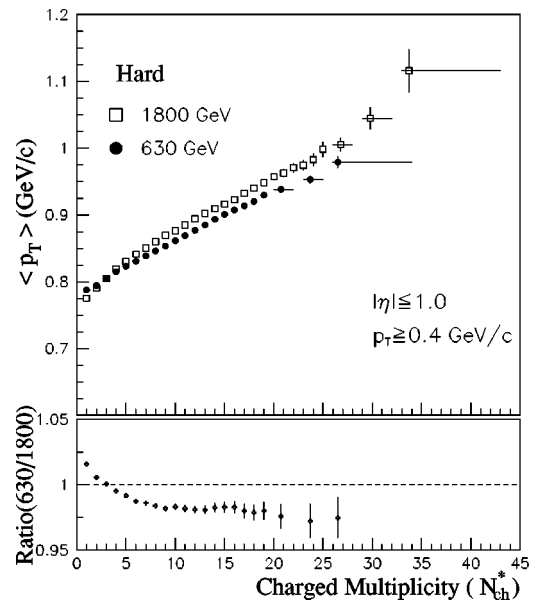


FIG. 13. Same as Fig. 11 for the *hard* samples.

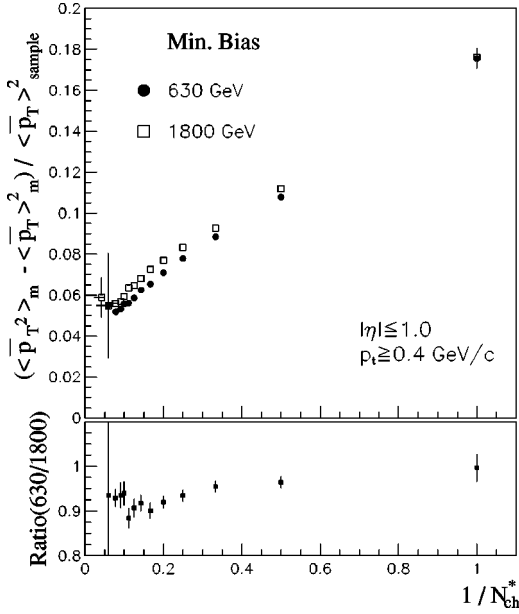


FIG. 14. Dispersion of the mean event p_T as a function of the inverse multiplicity for the full MB samples at 1800 and 630 GeV. At the bottom the ratio of the two curves is shown.

tion at fixed multiplicity in the “soft” sample is also energy invariant, a property which was unexpected. By this, we mean that the momentum distribution in the soft sample is determined only by the number of charged particles in the final state, independently of the center of mass energy.

The mean p_T as a function of the charged multiplicity in the soft samples scales remarkably well with energy. In addition, the mean p_T increases with multiplicity even in the soft sample where hard parton interactions are at most strongly suppressed. Neither feature is predicted by current theoretical or phenomenological models.

The dispersion of the $\langle p_T \rangle_{ev}$ shows a non-linear depen-

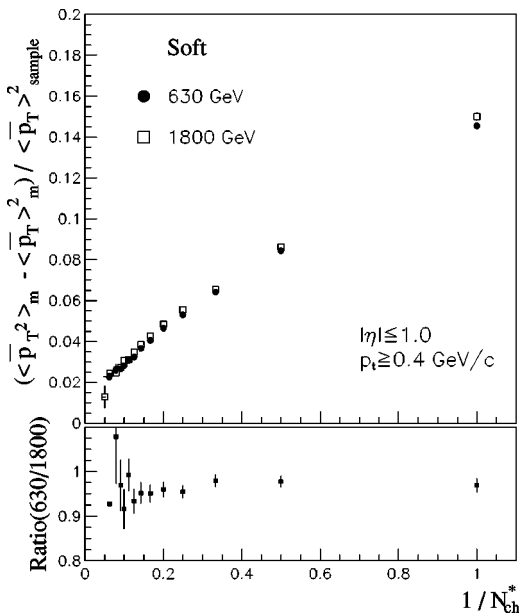


FIG. 15. Same as Fig. 14 for the *soft* samples.

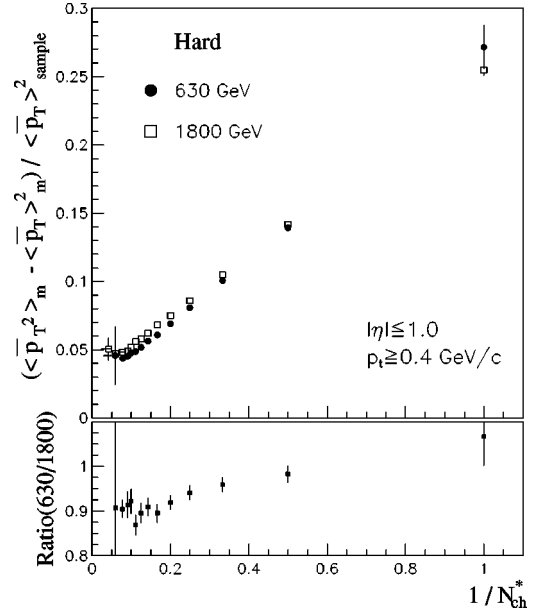


FIG. 16. Same as Fig. 14 for the *hard* samples.

dence on the inverse multiplicity, an observation not previously reported. The rise at multiplicity greater than ~ 10 is essentially due to the presence of hard parton interactions. In the same multiplicity region of the soft sample, the slope extrapolated to infinite multiplicity is consistent with zero. This would mean that asymptotically there are no dynamical correlations in the event mean p_T . The ratio of the dispersion in the soft sample at the two energies is flat as a function of multiplicity, a feature not exhibited by the hard sample.

All the distributions and correlations studied using the soft subsample are compatible with the hypothesis of invari-

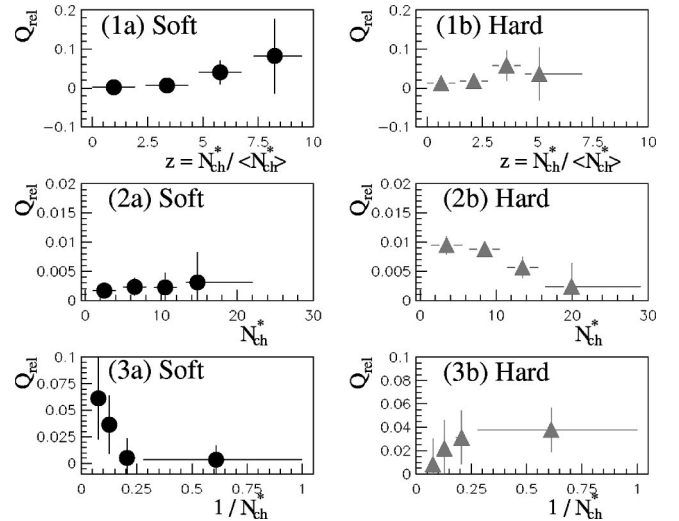


FIG. 17. The quantity plotted here is $Q_{rel} = (R_{(E_T=3)} - R)/R$. In Figs. 1a and 1b (respectively soft and hard samples) R is the ratio of the multiplicity distribution at the two energies with the standard cluster energy threshold ($E_T = 1.1 \text{ GeV}$). $R_{E_T=3}$ is the same for a threshold of 3 GeV. In Figs. 2a and 2b the same is done for the correlation of $\langle p_T \rangle$ versus multiplicity and in Figs. 3a and 3b for the $\langle p_T \rangle_{ev}$ dispersion.

ance with the center of mass energy, which is a new result. We conclude that the dynamical mechanism of inelastic multiparticle production in soft interactions, at least in this energy interval, is invariant with center of mass energy, and that the properties of the final state are determined only by the number of (charged) particles.

ACKNOWLEDGMENTS

We thank the Fermilab staff and the technical staffs of the participating institutions for their vital contributions. This work was supported by the U.S. Department of Energy and National Science Foundation, the Italian Istituto Nazionale di Fisica Nucleare, the Ministry of Education, Science, Sports and Culture of Japan, the Natural Sciences and Engineering Research Council of Canada, the National Science Council of the Republic of China, the Swiss National Science Foundation, the A. P. Sloan Foundation, the Bundesministerium fuer Bildung und Forschung, Germany, and the Korea Science and Engineering Foundation.

APPENDIX

The description of the settings of Monte Carlo generators refers to [22].

PYTHIA setting 1. The generator was tuned to best match

the data multiplicity and p_T distributions. The following parameters were changed with respect to the default MB configuration:

QCD high p_T processes plus “low- p_T ” production.

Second order running α_s .

Inclusion of K factors in hard cross sections for parton-parton interactions. A factor is introduced by a shift in the α_s , Q^2 argument.

Allow multiple parton-parton interactions.

Assume a varying impact parameter for multiple interactions and a hadronic matter overlap consistent with a double Gaussian matter distribution.

Fraction of the total hadronic matter contained in the core radius of the double Gaussian matter distribution inside the colliding hadrons equal to 0.2.

Core radius–main radius of the double Gaussian matter distribution inside the colliding hadrons equal to 0.5.

PYTHIA setting 2. Default MB configuration with effective minimum transverse momentum $p_{Tmin} = 1.4$ GeV/c.

PYTHIA setting 3. Default MB configuration with effective minimum transverse momentum $p_{Tmin} = 1.9$ GeV/c.

HERWIG setting 1. Default MB soft hadron-hadron events.

HERWIG setting 2. Default QCD $2 \rightarrow 2$ hard parton scattering with underlying multiplicity enhancement factor equal to 4.

-
- [1] R. Ansari *et al.*, *Z. Phys. C* **36**, 175 (1987); X. Wang and R.C. Hwa, *Phys. Rev. D* **39**, 187 (1989); UA1 Collaboration, F. Ceradini, *Proceedings of the Bari Europhysics Conference on HEP*, Bari, 1985 (Laterza, Bari, 1985).
- [2] T. Sjöstrand and M. van Zijl, *Phys. Rev. D* **36**, 2019 (1987), and references therein.
- [3] A summary of the references to these models can be found in [2].
- [4] F. Abe *et al.*, *Nucl. Instrum. Methods Phys. Res. A* **271**, 387 (1988), and references therein.
- [5] F. Abe *et al.*, *Phys. Rev. D* **52**, 4784 (1995).
- [6] F. Bedeschi *et al.*, *Nucl. Instrum. Methods Phys. Res. A* **268**, 50 (1988).
- [7] F. Snider *et al.*, *Nucl. Instrum. Methods Phys. Res. A* **268**, 75 (1988).
- [8] F. Balka *et al.*, *Nucl. Instrum. Methods Phys. Res. A* **267**, 272 (1988); S.R. Hahn *et al.*, *ibid.* **267**, 351 (1988); K. Yasuoka *et al.*, *ibid.* **267**, 315 (1988); R.G. Wagner *et al.*, *ibid.* **267**, 330 (1988); T. Devlin *et al.*, *ibid.* **267**, 24 (1988); S. Bertolucci *et al.*, *ibid.* **267**, 301 (1988); Y. Fukui *et al.*, *ibid.* **267**, 280 (1988); S. Cihangir *et al.*, *ibid.* **267**, 249 (1988); G. Brandenburg *et al.*, *ibid.* **267**, 257 (1988).
- [9] F. Abe *et al.*, *Phys. Rev. D* **56**, 3811 (1997); *Phys. Rev. Lett.* **79**, 584 (1997); X. Wang, *Phys. Rev. D* **46**, 1900 (1992); UA1 Collaboration, C. Albajar *et al.*, *Nucl. Phys.* **B309**, 405 (1988).
- [10] F. Abe *et al.*, *Phys. Rev. Lett.* **61**, 1819 (1988).
- [11] F. Abe *et al.*, *Phys. Rev. Lett.* **76**, 2015 (1996).
- [12] F. Abe *et al.*, *Phys. Rev. D* **58**, 072001 (1998).
- [13] Z. Koba, H.B. Nielsen, and P. Olesen, *Nucl. Phys.* **B40**, 317 (1972).
- [14] UA5 Collaboration, R.E. Ansorge *et al.*, *Z. Phys. C* **43**, 357 (1989); K. Alpgard *et al.*, *Phys. Lett.* **121B**, 209 (1983).
- [15] E735 Collaboration, T. Alexopoulos *et al.*, *Phys. Lett. B* **336**, 599 (1994); *Phys. Rev. Lett.* **60**, 1622 (1988); N. Moggi, *Nucl. Phys. B (Proc. Suppl.)* **71**, 221 (1999).
- [16] UA1 Collaboration, G. Arnison *et al.*, *Phys. Lett.* **118B**, 167 (1982).
- [17] A. Breakstone *et al.*, *Phys. Lett.* **132B**, 463 (1983); *Phys. Lett. B* **183**, 227 (1987); *Z. Phys. C* **33**, 333 (1987).
- [18] E735 Collaboration, T. Alexopoulos *et al.*, *Phys. Rev. D* **48**, 984 (1993); S.H. Oh, *Nucl. Phys. B (Proc. Suppl.)* **25**, 40 (1992).
- [19] S. Barshay, *Phys. Lett.* **127B**, 129 (1983).
- [20] L. Van Hove, *Phys. Lett.* **127B**, 138 (1982); R. Hagedorn, *Riv. Nuovo Cimento* **6**, 10 (1983); J.D. Bjorken, *Phys. Rev. D* **27**, 140 (1983).
- [21] X. Wang and C. Hwa, *Phys. Rev. D* **39**, 187 (1989); M. Jacob, CERN Report No. CERN/TH. 3515, 1983; F.W. Bopp, P. Aurenche, and J. Ranft, *Phys. Rev. D* **33**, 1867 (1986).
- [22] T. Sjöstrand, *Comput. Phys. Commun.* **82**, 74 (1994); G. Marchesini, B.R. Webber, G. Abbiendi, I.G. Knowles, M.H. Seymour, and L. Stanco, *ibid.* **67**, 465 (1992).
- [23] K. Braune *et al.*, *Phys. Lett.* **123B**, 467 (1983).
- [24] H. Appelshäuser, *Phys. Lett. B* **459**, 679 (1999).
- [25] M.L. Cherry *et al.*, *Acta Phys. Pol. B* **29**, 2129 (1998).
- [26] M. Gaździcki, *Eur. Phys. J. C* **6**, 365 (1999), and references therein.
- [27] F. Liu, *Eur. Phys. J. C* **8**, 649 (1999).
- [28] T.A. Trainor, *Nucl. Phys. B (Proc. Suppl.)* **92**, 16 (2001); H. C. Eggers and K. Fialkowski, *Proceedings of the ISMD 2000*, Tihany (Ungary), 2000 (World Scientific, Singapore, 2001).